Monthly Notices of the ROYAL ASTRONOMICAL SOCIETY

MNRAS **527,** L47–L53 (2024) https://doi.org/10.1093/mnrasl/slad145
Advance Access publication 2023 October 14

AT2023fhn (the Finch): a luminous fast blue optical transient at a large offset from its host galaxy

A. A. Chrimes [1,2★] P. G. Jonker,[2,3] A. J. Levan,[2,4] D. L. Coppejans,[4] N. Gaspari [2] B. P. Gompertz [5] P. J. Groot,[2,6,7] D. B. Malesani [2,8,9] A. Mummery,[10] E. R. Stanway [4] and K. Wiersema [11]

[1]*European Space Research and Technology Centre (ESTEC), European Space Agency (ESA), Keplerlaan 1, NL-2201 AZ Noordwijk, the Netherlands*
[2]*Department of Astrophysics/IMAPP, Radboud University, PO Box 9010, NL-6500 GL Nijmegen, the Netherlands*
[3]*SRON, Netherlands Institute for Space Research, Niels Bohrweg 4, NL-2333 CA Leiden, the Netherlands*
[4]*Department of Physics, University of Warwick, Gibbet Hill Road, Coventry CV4 7AL, UK*
[5]*Institute of Gravitational Wave Astronomy and School of Physics and Astronomy, University of Birmingham, Birmingham B15 2TT, UK*
[6]*Inter-University Institute for Data Intensive Astronomy, Department of Astronomy, University of Cape Town, Private Bag X3, Rondebosch 7701, South Africa*
[7]*South African Astronomical Observatory, P.O. Box 9, 7935 Observatory, South Africa*
[8]*Cosmic Dawn Center (DAWN), Denmark*
[9]*Niels Bohr Institute, University of Copenhagen, Jagtvej 128, DK-2200 Copenhagen N, Denmark*
[10]*Oxford Astrophysics, Denys Wilkinson Building, Keble Road, Oxford OX1 3RH, UK*
[11]*Centre for Astrophysics Research, University of Hertfordshire, Hatfield AL10 9AB, UK*

Accepted 2023 October 3. Received 2023 October 3; in original form 2023 July 4

ABSTRACT

Luminous fast blue optical transients (LFBOTs) – the prototypical example being AT 2018cow – are a rare class of events whose origins are poorly understood. They are characterized by rapid evolution, featureless blue spectra at early times, and luminous X-ray and radio emission. LFBOTs thus far have been found exclusively at small projected offsets from star-forming host galaxies. We present *Hubble Space Telescope*, Gemini, *Chandra*, and Very Large Array observations of a new LFBOT, AT 2023fhn. The *Hubble Space Telescope* data reveal a large offset (>3.5 half-light radii) from the two closest galaxies, both at redshift $z \sim 0.24$. The location of AT 2023fhn is in stark contrast with previous events, and demonstrates that LFBOTs can occur in a range of galactic environments.

Key words: supernovae: individual: AT 2023fhn – transients: supernovae – transients: tidal disruption events.

1 INTRODUCTION

The development of wide-field, high cadence and deep optical surveys in recent years – including the Zwicky Transient Facility (ZTF; Bellm et al. 2019), Asteroid Terrestrial-impact Last Alert System (Tonry et al. 2018), Panoramic Survey Telescope and Rapid Response System (Chambers et al. 2016), Gravitational-wave Optical Transient Observer (Steeghs et al. 2022), and Black hole Gravitational-wave Electromagnetic counterpart array (Bloemen et al. 2016), to name a few – is leading to ever more transient detections in the extremes of parameter space. This trend is set to continue with the Vera Rubin Observatory (LSST Science Collaboration 2009). Such surveys led to the discovery of fast blue optical transients (FBOTs), first identified as a class by Drout et al. (2014) in ZTF. FBOTs rise and fade on time-scales of days, and have (early-time) $g - r$ colours of −0.3 or bluer. These events also have featureless, blackbody-like spectra at early times with inferred temperatures $>10^4$ K (Pursiainen et al. 2018). It has since become clear that the majority are infant supernovae with low ejecta masses (Pursiainen et al. 2018), but a small number fade too rapidly to be powered by Ni-56 decay (faster than 0.2–0.3 mag per day), have peak absolute magnitudes rivalling SLSNe (<−20), and have accompanying luminous X-ray and radio emission. These bright, multiwavelength FBOTs have been dubbed luminous-FBOTs (LFBOTS; Metzger 2022), the first example of which is AT 2018cow ('the Cow', Prentice et al. 2018; Margutti et al. 2019; Perley et al. 2019). Since AT 2018cow, several other LFBOTs have been discovered (both in real time and archival searches), with varying degrees of multiwavelength coverage. These include ZTF18abvkwla ('the Koala', Ho et al. 2020), CSS161010 (Coppejans et al. 2020), ZTF20acigmel ('the Camel', Perley et al. 2021; Bright et al. 2022; Ho et al. 2022c), AT2020mrf (Yao et al. 2022), and AT 2022tsd ('the Tasmanian Devil', Ho et al. 2022a; Matthews et al. 2023). There are also a number of other lower confidence candidates (e.g. Ho et al. 2022b; Jiang et al. 2022; Perley et al. 2023). Despite the growing number of LFBOT discoveries, these events are intrinsically rare – the volumetric rate of AT 2018cow-like LFBOTs is estimated to be no more than 0.1 per cent of the local supernova rate (Ho et al. 2023b).

The nature of LFBOTs remains unclear. The time-scale of their light-curve evolution, X-ray and radio luminosity, late-time ultraviolet (UV) emission in the case of AT 2018cow (Sun et al. 2022; Chen et al. 2023a; Inkenhaag et al. 2023; Sun et al. 2023), and preference for star-forming dwarf and spiral hosts have proved challenging to explain with a single self-consistent model. Circumstellar medium interactions around young supernovae are a plausible origin for the early-time spectra and X-ray/radio emission of some FBOTs

★ E-mail: ashley.chrimes@esa.int

(Pursiainen et al. 2018; Ho et al. 2023b), as well as for the optical polarization behaviour (Maund et al. 2023). However, the peak absolute magnitude, rapid subsequent fading, high radio/X-ray luminosity, and peculiar optical and radio polarization of LFBOTs (Huang et al. 2019; Maund et al. 2023) require an alternative explanation. Following AT 2018cow, a few main classes of model emerged. These include central engines born in low-ejecta core-collapse events, powered by black hole accretion or magnetar spin-down (e.g. Margutti et al. 2019; Perley et al. 2019); mergers of stellar-mass black holes and hydrogen-poor stars (e.g. Metzger 2022); or the tidal disruption of a main-sequence star (Perley et al. 2019) or white dwarf by an intermediate-mass black hole (IMBH; Kuin et al. 2019). The former is motivated by the rapid light-curve decay and multiwavelength evolution which severely limits the possible ejecta mass; the latter two also by the time-scale – which is too fast for a supermassive black hole tidal disruption event (TDE) – and the weak (initially absent) hydrogen lines in the spectra. Many of these scenarios face challenges. For example, a magnetar central engine can power the early- or late-time UV emission in AT 2018cow, but not both (Chen et al. 2023b), while the environments of LFBOTS thus far – at small offsets within star-forming dwarfs and spirals, and with high circumstellar densities (Margutti et al. 2019) – favour a short-lived, massive star progenitor over an IMBH TDE. Further insight will come from similarly detailed studies of other LFBOTs, to establish which features are common to all objects in this class, and to understand the variety among them.

In this letter, we present multiwavelength observations of a new LFBOT, AT2023fhn ('the Finch'). The transient is significantly offset from the nearest galaxies, representing a deviation in terms of its environment from previous LFBOTs. This letter is structured as follows. In Section 2, we review how AT 2023fhn was discovered, and present early-time X-ray and radio observations. Section 3 presents follow-up observations, including *Hubble Space Telescope* (*HST*) imaging and Gemini spectroscopy. In Section 4, we discuss possible interpretations, and conclusions are drawn in Section 5. We adopt a cosmology with $H_0 = 69.6\,\mathrm{km\,s^{-1}\,Mpc^{-1}}$, $\Omega_\mathrm{m} = 0.29$, and $\Omega_\Lambda = 0.71$ (Wright 2006; Bennett et al. 2014). Uncertainties are given as 1σ unless otherwise stated, and magnitudes are quoted in the AB system (Oke & Gunn 1982).

2 DISCOVERY AND CLASSIFICATION

2.1 Early photometry and spectra

AT 2023fhn was discovered on 2023 April 10 with $m(r) = 19.74$ by ZTF (Fremling 2023). The blue colour of $g - r \sim -0.47$ and rapid $\sim$0.2 mag day^{-1} evolution immediately classified AT 2023fhn as an LFBOT candidate. Ho et al. (2023a) subsequently obtained Gemini GMOS-S spectroscopy of AT 2023fhn on 2023 April 19 (programme GS-2023A-Q-127), finding a featureless blue spectrum. On 2023 April 20, they obtained a spectrum of the nearby spiral galaxy ($\sim$5 arcsec offset), yielding a redshift of $z \sim 0.24$. At this redshift, the earliest ZTF g-band (12 April 2023) absolute magnitude is -21.5.

2.2 X-ray and radio observations

We triggered *Chandra X-ray Observatory* observations (PI: Chrimes; programme 24500143; Obs ID 26624), which were obtained on 2023 April 25 (06:58:08–15:46:51 UT). The faint-mode ACIS-S exposure lasted 30 ks. The data were reduced and analysed with standard CIAO (v4.13, caldb v4.9.3) procedures including reprocessing, filtering, and source measurement with SRCFLUX. Assuming a power law with a photon index $\Gamma = 2$ (Rivera Sandoval et al. 2018; Matthews et al. 2023), the unabsorbed source flux after correction for the Galactic neutral hydrogen column density of $NH = 2.4 \times 10^{20}\mathrm{cm^{-2}}$ (Kalberla et al. 2005) is $7.6^{-1.8}_{+2.2} \times 10^{-15}\,\mathrm{erg\,cm^{-2}\,s^{-1}}$ (0.5–7.0 keV). At the redshift of the spiral, this corresponds to a luminosity of $1.3^{-0.3}_{+0.4} \times 10^{42}\,\mathrm{erg\,s^{-1}}$, comparable to other LFBOTs at the same epoch (Rivera Sandoval et al. 2018; Kuin et al. 2019; Margutti et al. 2019; Coppejans et al. 2020; Bright et al. 2022; Yao et al. 2022; Matthews et al. 2023).

Table 1. VLA flux density upper limits. These are given as 3 times the local RMS. The third column lists the bandwidth. The final column lists limits on the luminosity, assuming a redshift of $z = 0.238$ (see Section 3.2).

Start date JD-2460056	Freq. (GHz)	BW (GHz)	T_exp (Min.)	Upper limit (μJy beam^{-1})	Upper limit (10^{28} erg s^{-1} Hz^{-1})
0.80733	1.50	1.024	35.9	130	22.5
0.78309	3.00	2.048	30.0	35	6.0
0.76507	6.05	2.048	21.0	18	3.1
0.74688	10.00	4.096	21.1	18	3.1
0.72090	15.02	6.144	30.1	11	1.9
0.69229	21.94	8.192	28.2	17	2.9
0.66552	32.94	8.192	25.4	25	4.3

Early radio observations (within a few weeks of discovery) produced non-detections, including a 10 GHz Northern Extended Millimetre Array upper limit of $2 \times 10^{29}\,\mathrm{erg\,s^{-1}\,Hz^{-1}}$ on the luminosity (Ho 2023), and upper limits from our own programme (SC240143, PI: Chrimes) on the Karl G. Jansky Very Large Array (VLA). We observed AT 2023fhn on 2023 April 22 ($\approx$12 d post detection) in standard phase-referencing mode using 3C286 as a flux density and bandpass calibrator, with J1014+2301 and J1016+2037 as complex gain calibrators. The observations were calibrated using the VLA Calibration Pipeline 2022.2.0.64 in CASA version 6.4.1 with additional manual flagging. We imaged the data using the task TCLEAN in CASA with Briggs weighting with a robust parameter of 1. No significant emission was detected at the source location. We provide the upper limits in Table 1. These early-time non-detections are consistent with the behaviour of previous LFBOTs. The transient was subsequently detected with the VLA on 2023 June 15 (Ho 2023) with luminosity $7.6 \times 10^{28}\,\mathrm{erg\,s^{-1}\,Hz^{-1}}$ (at 10 GHz), also similar to other LFBOTs at the same epoch (e.g. Margutti et al. 2019; Coppejans et al. 2020). The rapid evolution (time-scale of a few days) and peak optical absolute magnitude of -21.5 places AT 2023fhn firmly within the LFBOT region of time-scale/peak luminosity parameter space (see figs 3 and 14 of Ho et al. 2023b). Along with the hot featureless optical spectrum, X-ray, and radio detections, AT 2023fhn is unambiguously identified as a new AT 2018cow-like LFBOT.

3 FOLLOW-UP OBSERVATIONS

3.1 Hubble Space Telescope Imaging

3.1.1 Data reduction and photometry

HST WFC3/UVIS observations were taken with the *F555W* and *F814W* filters on 2023 May 17 (PI: Chrimes; proposal ID 17238). Three 364 s exposures with sub-pixel dithers were taken in each filter. The *F555W* exposures began 09:02:23 and ended 09:23:41 UT, the *F814W* exposures began 09:25:31 and ended 09:48:13 UT. The

_FLC images were combined using ASTRODRIZZLE[1] (Fruchter & Hook 2002), with PIX_FRAC = 0.8 and a final pixel scale of 0.025 arcsec pixel^{-1}. The transient is clearly identified in the reduced images, as shown in Fig. 1. Two adjacent galaxies are fully resolved: a barred spiral to the south and a dwarf/irregular to the southeast. These galaxies have Sloan Digital Sky Survey (SDSS) data release 16 (Ahumada et al. 2020) IDs SDSS J100803.73+210422.5 and SDSS J100803.87+210425.8. We perform photometry on AT 2023fhn with three methods. The first two use standard PHOTUTILS aperture photometry procedures in PYTHON (Bradley et al. 2021), but the background level is calculated in two ways. The first uses the MEDIANBACKGROUND estimator (using the whole image for the estimate). The second uses an annulus around the source (inner and outer radii of 1.5 and 4 times the aperture radius, and pixel values in the annulus clipped at $\pm 3\sigma$). For each of these background estimations, two aperture sizes are used – 2 and 0.4 arcsec – with the appropriate aperture corrections for *F555W* and *F814W* applied[2] AB magnitudes are derived from the PHOTFLAM and PHOTPLAM header values and the published conversion procedures.[3] For the third method, we use DOLPHOT (v2.0, Dolphin 2000). DOLPHOT performs point spread function (PSF) photometry on each _FLC image separately; these measurements are combined to give the reported value and its error. DOLPHOT provides instrumental magnitudes in the Vega system, but we instead report AB magnitudes using conversions calculated with STSYNPHOT (STScI Development Team 2020). Magnitude measurements for each combination of filter and methodology are given in Table 2. Smaller apertures and annulus background subtraction results in fainter magnitudes, indicative of the presence of diffuse emission around the transient (as can be seen in Fig. 1, see insets).

3.1.2 *Galaxy offsets and enclosed flux radii*

The sky-projected spatial offset of a transient from its host is a key piece of information for understanding its origin. Host-normalized offsets, offsets divided by the half-light radius of the host, are widely used in the literature (see Fig. 4) as they account for the projected extent of the host galaxy. In order to measure the offsets and host-normalized offsets of AT 2023fhn from the two nearby galaxies, we measure their centroids and half-light radii r_{50} (from Petrosian profile fitting) using the PYTHON package STATMORPH (Rodriguez-Gomez et al. 2019). We require objects to have at least five adjacent pixels, each $>1\sigma$ above the background. The resultant segmentation maps are convolved with a uniform filter of size 10 pixels and these filtered segmentation maps are used to identify objects by requiring values >0.5. Enclosed flux measurements are not restricted to the galaxy-associated pixels identified with this method; flux is measured out to $r_{\rm max}$ which extends beyond the segmentation area to the faint outer regions (further than twice then Petrosian radius, for details see Rodriguez-Gomez et al. 2019). We note that the transient lies outside the pixels selected as associated with the galaxy in both cases. Segmentation maps, radial light profiles in the direction of the transient, and STATMORPH Sérsic fits for the two galaxies in each filter, are provided in the associated github repository.[4]

[1]Part of DRIZZLEPAC, http://drizzlepac.stsci.edu/
[2]https://hubblesite.org/sites/www/home/hst/instrumentation/wfc3/data-analysis/photometric-calibration/uvis-encircled-energy
[3]https://hst-docs.stsci.edu/wfc3dhb/chapter-9-wfc3-data-analysis/9-1-photometry
[4]https://github.com/achrimes2/Finch

At $z = 0.238$ – the redshift of the spiral (and its satellite, see Section 3.2) – the physical scale is 3.80 kpc arcsec^{-1}. From the centre of the spiral, the projected offset of AT 2023fhn δr is 16.51 ± 0.09 kpc. From the centre of the satellite, the offset is 5.35 ± 0.06 kpc (uncertainties as described below). The non-parametric half-light radius r_{50} (enclosing 50 per cent of the flux, r_{50}) is measured to be 4.5 ± 0.2 kpc in *F555W* for the spiral. Given the satellite's ellipticity of 0.4 and the orientation of AT 2023fhn, we take r_{50} along the semimajor axis, which is 1.48 ± 0.10 kpc in *F555W*. In *F814W*, these values are 3.90 ± 0.13 and 1.29 ± 0.10 kpc, respectively. This corresponds to host-normalized offsets ($r_{\rm n} = \delta r / r_{50}$) of 3.7 ± 0.2 and 3.6 ± 0.2 in *F555W*, while in *F814W*, $r_{\rm n} = 4.25 \pm 0.14$ and 4.1 ± 0.3 (for the spiral and satellite, respectively). The quoted offset uncertainties are the quadrature sum of the transient positional uncertainty (given by FWHM/(2.35 × SNR), where FWHM is the full width at half-maximum and SNR is the signal-to-noise ratio) and the uncertainty on the galaxy centroids ($x_{\rm c}$, $y_{\rm c}$). The centroid uncertainties are calculated by resampling the input _FLC image set 100 times using their [ERR] extensions, redrizzling each resampled set, and measuring the morphological properties with STATMORPH on each iteration of the redrizzled image (see Lyman et al. 2017; Chrimes et al. 2019). The mean and standard deviation of the resultant $x_{\rm c}$, $y_{\rm c}$, and r_{50} distributions are used, along with the AT 2023fhn positional uncertainties, to calculate the values and their uncertainties quoted above.

3.1.3 *Search for underlying and extended emission*

Given the apparently isolated location of AT 2023fhn, it is prudent to search for any underlying (extended) emission at the transient location, such as a knot of star formation, cluster, or background galaxy. To establish whether the emission is unresolved, we first select a reference point source in the image (the object at coordinates $\alpha = 10^{\rm h}08^{\rm m}03.13^{\rm s}$, $\delta = +21^{\rm d}04^{\rm m}22.8^{\rm s}$). Cutouts around AT 2023fhn and the reference star are interpolated on to a pixel grid with twice the resolution (enabling sub-pixel shifts), before subtraction of the reference image from the one containing AT 2023fhn. The reference is scaled in peak flux and shifted in x, y to minimize the standard deviation at the location of AT 2023fhn in the residual image. The transient, reference, and residual images are shown in Fig. 2. To determine if the residuals are consistent with a clean point source subtraction, we perform PHOTUTILS aperture photometry (with an annulus) as described above. No significant residual flux is detected, demonstrating that any underlying (non-transient) source contributing significantly to the flux must be precisely co-located and also unresolved (the physical scale at this distance is 95 pc pixel^{-1}). Making use of Binary Population and Spectral Synthesis (BPASS v2.2; Eldridge et al. 2017; Stanway & Eldridge 2018) synthetic spectra, we calculate the maximum mass of a stellar cluster which can be present at the location of AT 2023fhn, without exceeding the observed luminosity in either *F555W* or *F814W*. We find that the maximum possible mass of an unresolved cluster rises with population age, from 3×10^6 M$_\odot$ at 10^6 yr to $\sim 10^9$ M$_\odot$ at 10^{10} yr. Therefore, the presence of a typical stellar cluster – at any age – cannot be ruled out. To search for extended emission, we smooth the images with a Gaussian filter ($\sigma = 1.5$) and scale them to show diffuse background light. The inset panels of Fig. 1 show cutouts of the smoothed and scaled images. Faint emission can be seen extending northwest of the satellite, plausibly a tidal stream. The surface brightness near the transient location (measured in a

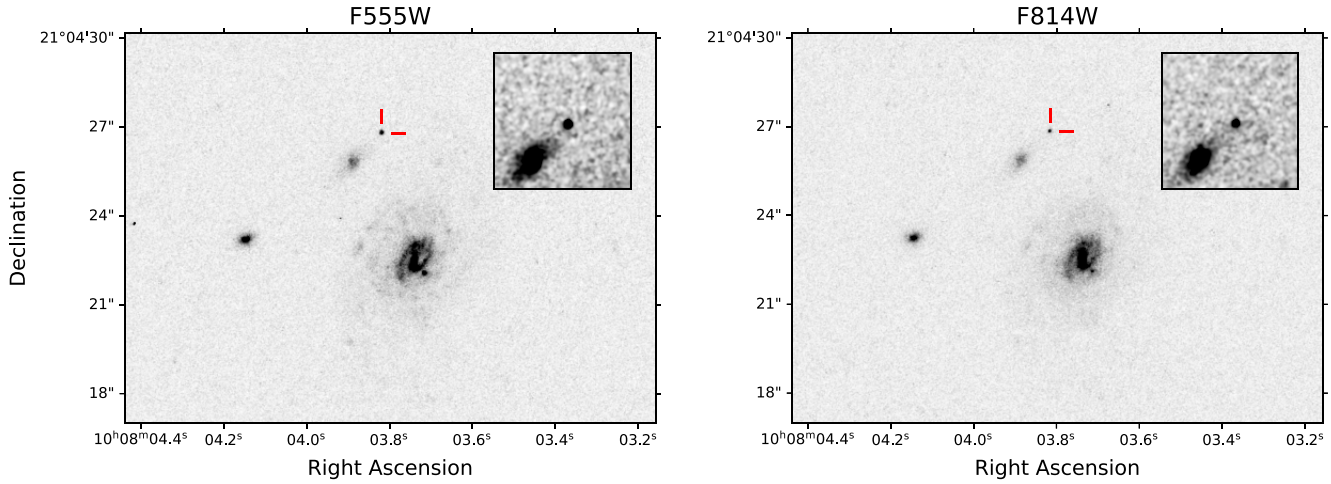

Figure 1. *HST* images of AT 2023fhn, indicated by red pointers, and the nearby host galaxy candidates. North is up and east is left in all images. The transient lies at a large offset from both the barred spiral to the south and the dwarf galaxy to the southeast. Smoothed and scaled 3.75 arcsec × 3.75 arcsec cutouts around AT 2023fhn are shown in the inset panels. The diffuse emission northwest of the dwarf (satellite) galaxy is an alternative parent stellar population.

Table 2. *HST* magnitudes m, and their uncertainties δm, for AT 2023fhn. In both filters, three photometry methods are listed – aperture photometry with median background estimation, aperture photometry with annulus background estimation, and DOLPHOT. For the non-DOLPHOT measurements, two aperture sizes (and hence enclosed energy corrections) are listed.

Filter	Method	Background	Aperture	m	δm
F555W	PHOTUTILS	Median	0.2″	24.31	0.02
F555W	PHOTUTILS	Annulus	0.2″	24.38	0.02
F555W	PHOTUTILS	Median	0.4″	24.13	0.03
F555W	PHOTUTILS	Annulus	0.4″	24.30	0.02
F555W	DOLPHOT	–	PSF	24.57	0.01
F814W	PHOTUTILS	Median	0.2″	24.17	0.03
F814W	PHOTUTILS	Annulus	0.2″	24.27	0.02
F814W	PHOTUTILS	Median	0.4″	23.94	0.04
F814W	PHOTUTILS	Annulus	0.4″	24.11	0.03
F814W	DOLPHOT	–	PSF	24.45	0.07

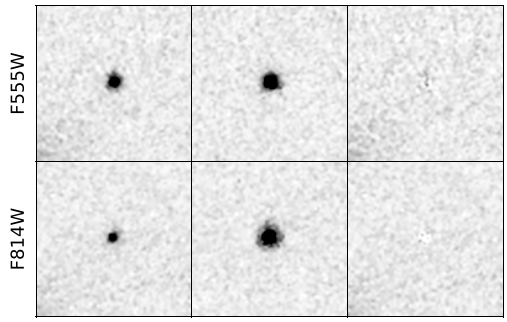

Figure 2. Subtraction of a reference star at the location of AT 2023fhn. The 2 arcsec × 2 arcsec cutouts show the transient (left), the reference star (middle), and the residual (right), after interpolating on to a finer pixel scale and subtraction of the shifted and vertically scaled reference star. The emission is consistent with being a point source.

1 arcsec radius around AT 2023fhn) is 25.2 mag arcsec^{-2} in *F555W* and 24.6 mag arcsec^{-2} in *F814W*.

3.2 Gemini spectroscopy

We obtained two epochs of Gemini/GMOS-S spectroscopy on 2023 April 22/23 and 2023 May 12, ∼10 and ∼26 d post-discovery, respectively (PI: Chrimes, programme GS-2023A-DD-102). The first epoch consisted of 4 s × 500 s exposures with the R400 grating, 1 arcsec slit width, and two central wavelengths (two exposures at 520 nm and two at 565 nm). The second epoch consisted of 4 s × 1845 s exposures with the R400 grating, 1 arcsec slit, and central wavelength 675 nm. Data reduction was performed using the PYTHON package DRAGONS (Labrie et al. 2019). Associated arcs, flats, and bias frames were taken as part of the programme. Sky lines and unusable regions (e.g. due to the amplifier 5 failure[5]) are manually masked. We bin the pixels by a factor of 6 along the wavelength axis to increase the SNR, and combine the 520 and 565 nm centred spectra by taking the mean where they overlap. We correct for Galactic extinction by adopting $E(B-V) = 0.025$ (Schlafly & Finkbeiner 2011), and calculate the extinction at each wavelength with the PYTHONEXTINCTION (Barbary 2016) module assuming $R_V = 3.1$. For flux calibration, spectrophotometric standard stars observed with the closest-matching set-up were found in the Gemini archive. For the 525 nm data, we use spectra of EG274 (programme GS-2023A-FT-205), for the 565 nm data we use LTT6248 (GS-2022A-Q-315), and for the 675 nm data we use LTT1020 (GS-2022B-Q-126). The final extinction-corrected spectra are plotted in Fig. 3.

In our first epoch of spectroscopy (22/23 April), AT 2023fhn is detected as shown in Fig. 3. Fitting a blackbody to the Galactic extinction-corrected, rest-frame spectrum yields a temperature of $24.8^{+2.4}_{-2.3} \times 10^3$ K ($\chi^2_\nu = 3.66$ with 282 degrees of freedom, where uncertainties are derived from the local standard deviation of the spectrum). This compares with a temperature of $17.5^{+1.2}_{-1.0} \times 10^3$ K derived from FORS2 photometry taken on the following night (Wise & Perley 2023). The large χ^2_ν is likely due to correlated, systematic errors (e.g. from imperfect flux calibration) that have not been accounted for. A power law produces a fit of similar quality – taking $F_\lambda \propto \nu^{2-\beta}$, we find a best-fitting power-law index $\beta = -1.24^{+0.06}_{-0.09}$, with $\chi^2_\nu = 3.63$. Nevertheless, temperatures of $\sim 20 \times 10^3$ K are comparable to AT 2018cow, which had a blackbody temperature

[5] https://www.gemini.edu/node/21963

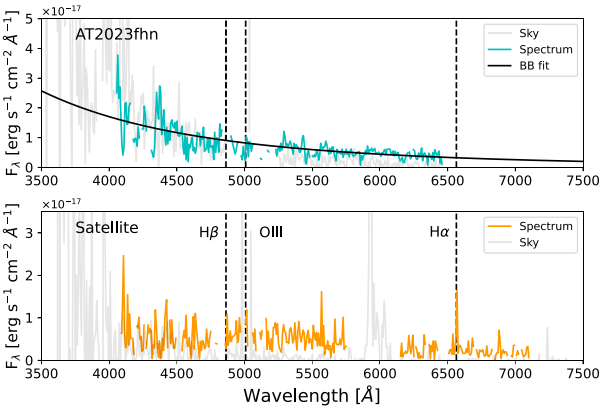

Figure 3. Upper panel: the background-subtracted spectrum of AT 2023fhn obtained with Gemini/GMOS-S on 2023 April 22/23, ∼10 rest-frame days post-discovery, and shifted into the transient rest frame. A blackbody fit returns $T = 24.8^{+2.4}_{-2.3} \times 10^3$ K. Background traces are shown in light grey. Lower panel: a spectrum of the satellite galaxy. A robust detection of the H α emission line at $z = 0.238 \pm 0.004$ confirms an association with the adjacent spiral.

of $19.3^{+0.7}_{-0.8} \times 10^3$ K at a similar rest-frame epoch (Prentice et al. 2018). No correction for host-intrinsic extinction has been made, however, as revealed in the *HST* imaging, the transient appears to be far away from any significant sources of dust, as it lies outside the bulk of the optical light of both nearby galaxies. In the second epoch of spectroscopy (12 May), the transient had faded sufficiently to result in a non-detection, with an upper limit on H α emission at its location (taking an aperture with the same radius as the seeing) of $<1.2 \times 10^{-16}$ erg s^{-1} cm^{-2}. The slit was also placed on the edge of the satellite galaxy. From the centroid and width of the H α line, we derive a redshift $z = 0.238 \pm 0.004$, consistent with the spiral redshift of ∼0.24 reported by Ho et al. (2023a), and backing up the satellite interpretation for this galaxy. We have adopted $z = 0.238$ for all relevant calculations in this letter.

4 DISCUSSION

All published LFBOTS to date have occurred in star-forming dwarfs (the Koala, CSS161010, the Camel, AT 2020mrf; Coppejans et al. 2020; Ho et al. 2020; Perley et al. 2021; Yao et al. 2022) or spirals (the Cow; Prentice et al. 2018; Lyman et al. 2020). AT 2023fhn also has a star-forming host, assuming one of the spiral or dwarf (both are strong H α emitters) is the galaxy of origin. However, in contrast with LFBOTs so far, it lies far away from the bulk of the host light for either choice of host galaxy. Such offsets are atypical for core-collapse transients due to the short (10–100 Myr lifetimes) of the progenitor stars. Fig. 4 compares the physical projected offsets and host-normalized offsets of a range of transients compiled from the literature, including long gamma-ray bursts (LGRBs), short gamma-ray bursts (SGRBs), superluminous supernovae (SLSNe), other core-collapse supernovae (CCSNe), fast radio bursts (FRBs), Ca-rich and type Ia SNe. The host offsets of four previous LFBOTs are also shown (r_n values were not reported for these events). AT 2023fhn lies much further out from its host than other LFBOTs to date. To quantify this, we randomly draw five (the number of LFBOTs with host offset measurements in Fig. 4) offsets from the Schulze et al. (2021) CCSN distribution 10^4 times, and calculate the frequency with which at least one of these lies at 5.35 (16.51) kpc or greater (for the satellite and spiral, respectively). For the satellite, this occurs in 85 per cent of random draws, for the spiral it occurs in 13 per cent. In terms of host-normalized offset, only ∼1 per cent of CCSNe occur at higher offsets than AT 2023fhn. In all 4 combinations of filter and galaxy choice, the transient lies outside the pixels selected as associated with the galaxies, therefore (by definition) the transient will have a fraction of light (Fruchter et al. 2006) value $F_{\rm light} = 0$ in both filters. This is unlikely but not unprecedented for core-collapse events; a few per cent of CCSN have $F_{\rm light} = 0$ (Svensson et al. 2010). Therefore, a core-collapse origin cannot be ruled out.

If originating at a lower offset, time-of-travel arguments require a massive star with velocity $\gtrsim$50/350 km s^{-1} for the spiral/satellite, assuming a long-lived 100 Myr-old progenitor (Eldridge, Stanway & Tang 2019) and an origin at $\sim r_{50}$. Only a small fraction of massive stars have such high velocities (e.g. Portegies Zwart 2000; de Wit et al. 2005; Eldridge, Langer & Tout 2011; Renzo et al. 2019; Chrimes et al. 2023). The delayed mergers of compact objects can also achieve high offsets (i.e. SGRBs), but the luminosity, spectra, and rapid evolution of LFBOTs effectively rule out an association with even the most extreme of these transients (e.g. Kann et al. 2011; Sarin et al. 2022). Since no spectroscopic redshift for the transient has been measured, we consider the probability of a chance alignment $P_{\rm chance}$ between AT 2023fhn and the two galaxies (following Bloom, Kulkarni & Djorgovski 2002; Berger 2010). $P_{\rm chance}$ is calculated using SDSS DR16 r-band magnitudes for the spiral and satellite, which are 18.94 ± 0.02 and 22.61 ± 0.14, respectively. For the spiral, we find $P_{\rm chance} = 0.78$ per cent, and for the satellite $P_{\rm chance} =$ 1.38 per cent. Therefore, AT 2023fhn is likely associated with one of the two galaxies. As shown in the inset panels of Fig. 1, the progenitor may have originated in a faint tidal stream or spiral arm. Based on our early-time radio and H α upper limits (Sections 2 and 3.2), and using the star formation rate (SFR) calibrations of Murphy et al. (2011), we derive 3σ upper limits on the underlying SFR at the location of AT 2023fhn of $\sim$6 M$_\odot$yr^{-1} (at 6.05 GHz, the strongest radio constraint) and $\sim$0.1 M$_\odot$yr^{-1} (H α). The *F555W* (rest frame ∼ *B* band) surface brightness of 25.2 mag arcsec^{-2} (Section 3.1.3) is among the faintest ∼2 per cent of (*u* band) local surface brightnesses for CCSNe (Kelly & Kirshner 2012). Unless the population is extremely young, adjusting for the *B*-band/*u*-band discrepancy would give an even fainter surface brightness (due to lower flux bluewards of the Balmer break). An IMBH TDE explanation requires an underlying cluster, since a dense stellar environment is necessary to make encounters likely (e.g. Ye, Fragione & Perna 2023). As shown in Section 3.1.3, a cluster at the location of AT 2023fhn cannot be ruled out. At $z \sim 0.24$, even the brightest and largest GCs would have optical apparent magnitudes of ∼30 – far fainter than the source in the *HST* images – and angular extents too small to be resolved (Harris 2010). Finally, we compare the offset of AT 2023fhn from the spiral with the distribution of GCs around M81 (which has a similar physical size and morphology), using the Sérsic distribution of Lomelí-Núñez et al. (2022) (see also Perelmuter & Racine 1995). The GC offsets, and distribution normalized by the *F555W* half-light radius of the spiral, are shown in Fig. 4. Only 0.5 per cent of GCs occur at the offset of AT 2023fhn or higher. While unlikely based on this statistic, the lack of strong photometric constraints mean that an origin in a GC is also not ruled out.

5 CONCLUSIONS

In this letter, we have presented *HST*, Gemini, *Chandra,* and VLA observations of AT 2023fhn, the first LFBOT to lie at a large offset from its host galaxy. Although the location is more representative of other transient types, given the offset, local surface brightness, limit on star formation, and constraints on an underlying cluster,

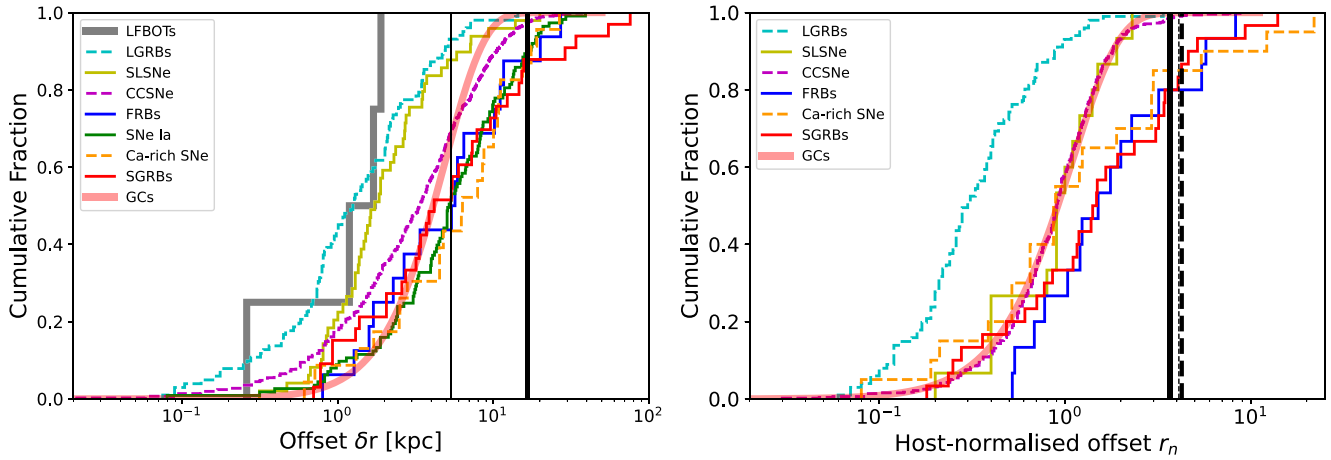

Figure 4. The cumulative offset and host-normalized offset distributions of a variety of transients, and the offset of AT 2023fhn from the spiral (thick black vertical lines) and its satellite (narrow vertical lines) – solid lines represent *F555W*, dashed lines *F814W*. The four previous LFBOT offsets are from Prentice et al. (2018, the Cow), Ho et al. (2020, the Koala), Coppejans et al. (2020, CSS161010), and Yao et al. (2022, AT 2020mrf). The comparison distributions are from Blanchard, Berger & Fong (2016), Lyman et al. (2017, LGRBs), Lunnan et al. (2015), Schulze et al. (2021, SLSNe), Kelly & Kirshner (2012), Schulze et al. (2021, CCSNe), Bhandari et al. (2022, FRBs), Wang et al. (2013, type Ia SNe), Lunnan et al. (2017), De et al. (2020, Ca-rich SNe), and Fong et al. (2022, SGRBs). Also shown is the globular cluster (GC) offset distribution around M81 (Lomelí-Núñez et al. 2022).

we cannot rule out a massive star progenitor. Likewise, a TDE in an unseen cluster cannot be ruled out. Environmental studies are needed for a population of LFBOTs to determine if AT 2023fhn is a significant outlier. Late-time imaging will put further constraints on the underlying stellar population, while detailed modelling of the spectra and multiwavelength light curve is needed to reveal more about the origin of this enigmatic transient.

ACKNOWLEDGEMENTS

This work is part of the research programme ATHENA with project number 184.034.002, which is (partly) financed by the Dutch Research Council (NWO). This research has made use of computing facilities provided by the Scientific Computing Research Technology Platform of the University of Warwick. Observations analysed in this work were taken by the NASA/ESA *HST* under programme 17238. This research has made use of software provided by the Chandra X-ray Center (CXC) in the application of the CIAO package (Fruscione et al. 2006). The National Radio Astronomy Observatory is a facility of the National Science Foundation operated under cooperative agreement by Associated Universities, Inc. Based on observations obtained at the international Gemini Observatory, a programme of NSF's NOIRLab, which is managed by the Association of Universities for Research in Astronomy (AURA) under a cooperative agreement with the National Science Foundation on behalf of the Gemini Observatory partnership. Finally, we thank the anonymous referee for their helpful feedback on this manuscript.

DATA AVAILABILITY

The data used are available upon request. Scripts and parameter files are available at https://github.com/achrimes2/Finch.

REFERENCES

Ahumada R. et al., 2020, ApJS, 249, 3
Barbary K., 2016, extinction v0.3.0
Bellm E. C. et al., 2019, PASP, 131, 018002
Bennett C. L., Larson D., Weiland J. L., Hinshaw G., 2014, ApJ, 794, 135
Berger E., 2010, ApJ, 722, 1946
Bhandari S. et al., 2022, AJ, 163, 69
Blanchard P. K., Berger E., Fong W.-f., 2016, ApJ, 817, 144
Bloemen S. et al., 2016, in Hall H. J., Gilmozzi R., Marshall H. K., eds, Proc. SPIE Conf. Ser. Vol. 9906, Ground-Based and Airborne Telescopes VI. SPIE, Bellingham, p. 990664
Bloom J. S., Kulkarni S. R., Djorgovski S. G., 2002, AJ, 123, 1111
Bradley L. et al., 2021, astropy/photutils: 1.1.0
Bright J. S. et al., 2022, ApJ, 926, 112
Chambers K. C. et al., 2016, preprint (arXiv:1612.05560)
Chen Y. et al., 2023a, ApJ, 955, 42
Chen Y., Drout M. R., Piro A. L., Kilpatrick C. D., Foley R. J., Rojas-Bravo C., Magee M. R., 2023b, ApJ, 955, 43
Chrimes A. A. et al., 2019, MNRAS, 486, 3105
Chrimes A. A. et al., 2023, MNRAS, 522, 2029
Coppejans D. L. et al., 2020, ApJ, 895, L23
De K. et al., 2020, ApJ, 905, 58
Dolphin A. E., 2000, PASP, 112, 1383
Drout M. R. et al., 2014, ApJ, 794, 23
de Wit W. J., Testi L., Palla F., Zinnecker H., 2005, A&A, 437, 247
Eldridge J. J., Langer N., Tout C. A., 2011, MNRAS, 414, 3501
Eldridge J. J., Stanway E. R., Xiao L., McClelland L. A. S., Taylor G., Ng M., Greis S. M. L., Bray J. C., 2017, Publ. Astron. Soc. Aust., 34, e058
Eldridge J. J., Stanway E. R., Tang P. N., 2019, MNRAS, 482, 870
Fong W.-f. et al., 2022, ApJ, 940, 56
Fremling C., 2023, Transient Name Serv. Discovery Rep., 2023-775, 1
Fruchter A. S., Hook R. N., 2002, PASP, 114, 144
Fruchter A. S. et al., 2006, Nature, 441, 463
Fruscione A. et al., 2006, in Silva D. R., Doxsey R. E., eds, Proc. SPIE Conf. Ser. Vol. 6270, Observatory Operations: Strategies, Processes, and Systems. SPIE, Bellingham, p. 62701V
Harris W. E., 2010, preprint (arXiv:1012.3224)
Ho A. Y. Q., 2023, Transient Name Serv. AstroNote, 174, 1
Ho A. Y. Q. et al., 2020, ApJ, 895, 49
Ho A. Y. Q., Perley D. A., Filippenko A. V., Zheng W., Brink T. G., Li M., Wang K., 2022a, Transient Name Serv. AstroNote, 199, 1
Ho A. Y. Q., Liu C., Chen P., Perley D., Wang K., Altunin I., 2022b, Transient Name Serv. AstroNote, 275, 1

Ho A. Y. Q. et al., 2022c, ApJ, 932, 116
Ho A. Y. Q., Liu C., Andreoni I., Coughlin M., Qin Y., Perley D., 2023a, Transient Name Serv. AstroNote, 93, 1
Ho A. Y. Q. et al., 2023b, ApJ, 949, 120
Huang K. et al., 2019, ApJ, 878, L25
Inkenhaag A., Jonker P. G., Levan A. J., Chrimes A. A., Mummery A., Perley D. A., Tanvir N. R., 2023, MNRAS, 525, 4042
Jiang J.-a. et al., 2022, ApJ, 933, L36
Kalberla P. M. W., Burton W. B., Hartmann D., Arnal E. M., Bajaja E., Morras R., Pöppel W. G. L., 2005, A&A, 440, 775
Kann D. A. et al., 2011, ApJ, 734, 96
Kelly P. L., Kirshner R. P., 2012, ApJ, 759, 107
Kuin N. P. M. et al., 2019, MNRAS, 487, 2505
Labrie K., Anderson K., Cárdenes R., Simpson C., Turner J. E. H., 2019, in Teuben P. J., Pound M. W., Thomas B. A., Warner E. M., eds, ASP Conf. Ser. Vol. 523, Astronomical Data Analysis Software and Systems XXVII. Astron. Soc. Pac., San Francisco, p. 321
Lomelí-Núñez L., Mayya Y. D., Rodríguez-Merino L. H., Ovando P. A., Rosa-González D., 2022, MNRAS, 509, 180
LSST Science Collaboration, 2009, preprint (arXiv:0912.0201)
Lunnan R. et al., 2015, ApJ, 804, 90
Lunnan R. et al., 2017, ApJ, 836, 60
Lyman J. D. et al., 2017, MNRAS, 467, 1795
Lyman J. D., Galbany L., Sánchez S. F., Anderson J. P., Kuncarayakti H., Prieto J. L., 2020, MNRAS, 495, 992
Margutti R. et al., 2019, ApJ, 872, 18
Matthews D. J. et al., 2023, Res. Notes Am. Astron. Soc., 7, 126
Maund J. R. et al., 2023, MNRAS, 521, 3323
Metzger B. D., 2022, ApJ, 932, 84
Murphy E. J. et al., 2011, ApJ, 737, 67
Oke J. B., Gunn J. E., 1982, PASP, 94, 586
Perelmuter J.-M., Racine R., 1995, AJ, 109, 1055
Perley D. A. et al., 2019, MNRAS, 484, 1031
Perley D. A. et al., 2021, MNRAS, 508, 5138
Perley D. A., Ho A. Y. Q., Hinds K., Jacobson-Galan W., 2023, Transient Name Serv. AstroNote, 41, 1
Portegies Zwart S. F., 2000, ApJ, 544, 437
Prentice S. J. et al., 2018, ApJ, 865, L3
Pursiainen M. et al., 2018, MNRAS, 481, 894
Renzo M. et al., 2019, A&A, 624, A66
Rivera Sandoval L. E., Maccarone T. J., Corsi A., Brown P. J., Pooley D., Wheeler J. C., 2018, MNRAS, 480, L146
Rodriguez-Gomez V. et al., 2019, MNRAS, 483, 4140
Sarin N., Omand C. M. B., Margalit B., Jones D. I., 2022, MNRAS, 516, 4949
Schlafly E. F., Finkbeiner D. P., 2011, ApJ, 737, 103
Schulze S. et al., 2021, ApJS, 255, 29
Stanway E. R., Eldridge J. J., 2018, MNRAS, 479, 75
Steeghs D. et al., 2022, MNRAS, 511, 2405
STScI Development Team, 2020, Astrophysics Source Code Library, record ascl:2010.003
Sun N.-C., Maund J. R., Crowther P. A., Liu L.-D., 2022, MNRAS, 512, L66
Sun N.-C., Maund J. R., Shao Y., Janiak I. A., 2023, MNRAS, 519, 3785
Svensson K. M., Levan A. J., Tanvir N. R., Fruchter A. S., Strolger L.-G., 2010, MNRAS, 405, 57
Tonry J. L. et al., 2018, PASP, 130, 064505
Wang X., Wang L., Filippenko A. V., Zhang T., Zhao X., 2013, Science, 340, 170
Wise J., Perley D., 2023, Transient Name Serv. AstroNote, 101, 1
Wright E. L., 2006, PASP, 118, 1711
Yao Y. et al., 2022, ApJ, 934, 104
Ye C. S., Fragione G., Perna R., 2023, ApJ, 953, 141

This paper has been typeset from a TEX/LATEX file prepared by the author.